PARAMETER CALIBRATION OF THE DISCRETE ELEMENT MODEL FOR THE AGRICULTURAL MACHINERY-LATERITIC SOIL-PANAX NOTOGINSENG INTERACTION DURING THE TRANSPLANTING PROCESS

/

三七移栽过程机具-红土-三七交互离散元模型参数标定

Wei SU[1], Yi ZENG [1], Qingxu YU*[2], Congcong LIAO[1], Qinghui LAI[1], Cantong SU[1]
[1]University of Science and Technology Kunming, Kunming 650093, China;
[2]Nanjing Institute of Agricultural Mechanization, Ministry of Agriculture and Rural Affairs, Nanjing 210014, China;
E-mail: yqx5205@163.com
** Correspondent authors: Qing xu YU*
DOI: https://doi.org/10.35633/inmateh-79-62

***Keywords:** Discrete element method; Parameter calibration; Notoginseng; laterite soil; JKR contact model*

ABSTRACT

This study calibrated key contact parameters for discrete element simulations of interactions among Panax notoginseng seedlings, lateritic soil, and 65Mn steel to address the lack of systematic multi-media parameter calibration methods. The researchers investigated three core contact interfaces using EDEM software, focusing on JKR surface energy, restitution coefficient, static friction coefficient, and rolling friction coefficient. They employed angle of repose tests, mixture collapse tests, and inclined plane rolling tests, combined with orthogonal design and response surface methodology, to establish correlation models between simulation and physical results. Through analysis of variance and multi-objective optimization, the team identified significant parameters and their optimal combinations for each interface. Validation showed that the optimized model exhibited relative errors below 7.5% across all tests, with prediction accuracy improved by over 30%. Field experiments further confirmed the model's reliability, providing theoretical support for structural optimization of Panax notoginseng transplanters.

摘要

为解决农业机械—红壤—作物相互作用离散元模拟中多介质接触参数缺乏系统标定方法的问题，本研究针对三七种苗—红壤、红壤—红壤、红壤—65Mn 钢三个核心接触界面，采用 EDEM 软件开展了关键接触参数标定优化研究。研究团队以 JKR 表面能、恢复系数、静摩擦系数和滚动摩擦系数为标定参数，采用休止角、混合坍塌、斜面滚动等物理试验，结合正交设计和响应面法，建立了模拟与物理试验的关联模型。通过方差分析和多目标优化，确定了各界面的显著参数及其最优组合。验证表明，优化后模型各项试验相对误差均低于 7.5%，预测精度提高 30% 以上。田间试验进一步证实了模型的可靠性，为三七移栽机结构优化提供了理论支撑。

INTRODUCTION

Panax notoginseng is a rare and valuable medicinal plant endemic to China, primarily cultivated in the southwestern regions including Yunnan, Guangxi, and Guizhou *(Liu et al., 2017; Yang et al., 2019*). Its dried roots and rhizomes have notable therapeutic effects. However, *P. notoginseng* transplantation faces challenges: tender seedlings are easily damaged during mechanical operations, reducing survival rates and yields. The cultivation soil for *P. notoginseng* is a cohesive lateritic soil characterized by poor workability, high moisture content, heavy texture, and high specific resistance (*Shao et al., 2006; Xing et al., 2020*). Such soil causes excessive resistance and severe adhesion, hindering Yunnan's *P. notoginseng* industry and mechanized transplantation development.

Discrete element method (*DEM*) simulation serves as a critical approach for investigating the coupled motion characteristics of the agricultural machinery–soil–seedling system, while accurate and reliable DEM parameters constitute the fundamental basis and prerequisite for studying the interaction characteristics of the agricultural machinery–lateritic soil–*P. notoginseng* system *(Aikins et al., 2021; Zeng et al., 2021*).

[1] *Wei SU, Ph. D. Professor; Qingxu YU, Ph. D. Assistant Researcher; Qinghui LAI, Ph. D. Professor; Yi ZENG, Master Candidate; Congcong LIAO, Master Candidate; Cantong SU, Master Candidate.*

Parameter calibration is a pivotal step in DEM simulations, as its accuracy directly governs the reliability of simulation results. The Johnson-Kendall-Roberts (*JKR*) contact model, capable of precisely characterizing cohesive interactions between particles, has been widely adopted in DEM modeling of cohesive soils. To date, researchers worldwide have conducted systematic studies on seedling–soil contact parameter calibration targeting crops such as corn, potato, and ginseng. *Tian Xinliang et al., (2021*) provided theoretical references for the discrete element simulation of corn straw–soil mixtures in black soil regions. *Xiang Wei et al., (2019*), based on soil accumulation tests, adopted the Hertz-Mindlin with JKR contact model to construct a discrete element simulation model of southern clayey soil. *Li Junwei et al., (2019)*, utilized the Hertz-Mindlin with JKR cohesion contact model in EDEM to calibrate clayey black soil with varying moisture contents in Northeast China, providing references for agricultural machinery operations under different moisture conditions. *Bahrami et al., (2020)*, employed the hysteretic spring–linear cohesion contact model to conduct DEM simulations of plate sinkage tests on cohesive soils with varying moisture contents, elucidating the influence of key parameters on sinkage characteristics. *Adajar et al., (2021)*, performed calibration of the residue–soil friction coefficient and restitution coefficient using the discrete element method, specifically targeting the crop residue–soil contact interface, thereby providing key parameter foundations for modeling soil–crop interactions under straw mulching conditions.

Although substantial progress has been achieved in agricultural DEM parameter calibration, a significant research gap remains regarding the systematic investigation of the distinctive tool–lateritic soil – *P. notoginseng* ternary system. This study focuses on *P. notoginseng* seedlings, southwestern lateritic soil, and 65Mn steel tools, with the primary objective of improving discrete element simulation accuracy. Adopting a methodology that couples physical experiments with simulation modeling, parameter calibration was conducted using three types of tests: angle of repose test, mixture collapse test, and inclined plane rolling test, to acquire fundamental physical data for multiple contact interfaces. A discrete element model was developed using EDEM software, and the JKR contact model was selected to characterize interparticle cohesion and friction behaviors. By integrating orthogonal experimental design with response surface methodology, correlation models between simulation outputs and physical test results were established. Iterative optimization was performed to determine the optimal values of JKR surface energy, coefficient of restitution, coefficient of static friction, and coefficient of rolling friction for all contact interfaces. The reliability of the calibrated model was ultimately validated through experimental verification. The research outcomes provide critical parameter support and theoretical foundations for optimizing the structural design of *P. notoginseng* transplanting machinery and precisely matching operational parameters, while simultaneously establishing a transferable technical framework for DEM parameter calibration in characteristic medicinal plant–regional soil systems.

MATERIALS AND METHODS

Material selection

Lateritic soil samples were collected from the core cultivation area of *P. notoginseng* in Wenshan Prefecture, Yunnan Province, which features typical lateritic soil well-suited for *P. notoginseng* cultivation (*You et al., 2022*). *P. notoginseng* seedling samples were obtained from a cultivation base in Wenshan. In accordance with the DB53/T 055.3-2020 standard for *P. notoginseng* seedlings (*Yunnan Provincial Administration for Market Regulation, 2020*), 30 robust and undamaged first-grade annual seedlings were selected.

a) *b)* *c)*

Fig. 1 – Experimental materials

a) P. notoginseng Transplanting Machine; b) Experimental laterite soil; C) P. notoginseng Seedlings for Experiment

Physical test determination of contact parameters

The mechanical behavior and motion characteristics involved in *P. notoginseng* transplantation are governed primarily by the contact parameters for soil–soil, soil–implement, and soil – *P. notoginseng* interactions. Therefore, these contact parameters were initially determined through physical experiments.

The coefficient of restitution (C_R) was determined in this study using the free-fall impact method (*Shi et al., 2020*), as illustrated in Figure 2.

$$C_R = \frac{V_1}{V_0} \tag{1}$$

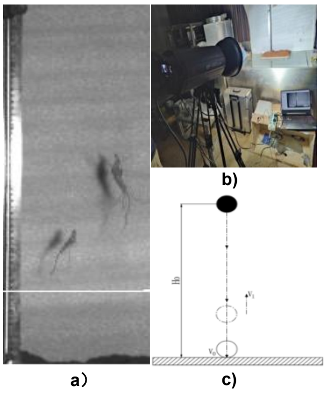

Fig. 2 – Measurement of the coefficient of restitution
a) High-speed photography; b) High-speed photographic setup; c) Schematic diagram of the coefficient of restitution (C_R)

The coefficient of *static friction (S_F)* was determined using the inclined plane method (*Aikins et al., 2021*), as shown in Figure 3.

$$S_F = \frac{F_1}{N_1} = \frac{G_1 \sin\theta_1}{G_1 \cos\theta_1} = \tan\theta_1 \tag{2}$$

where: F_1 is the friction force acting on the material specimen, *N;*
N_1 is the normal support force exerted on the specimen, *N;*
G_1 is the weight of the material specimen, *N;*
θ_1 is the inclination angle at which sliding begins, (°).

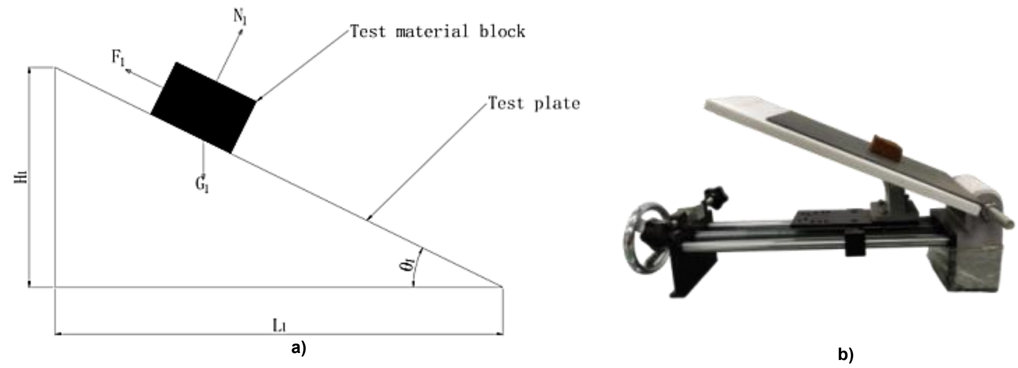

Fig. 3 – Measurement of the coefficient of static friction
a) Principle of static friction coefficient testing; b) Static friction coefficient test bench

The rolling friction coefficient (R_F) was determined using an angle adjustment device based on the principle of energy conservation (*Zhang et al., 2022*), as shown in Figure 4.

$$G_2 H_2 = R_F G_2 (G_2 \cos\theta_2 + L_2) \tag{3}$$

where: G_2 is the weight of the material sphere, *N;*
H_2 is the vertical distance between the material sphere and the horizontal plane, *mm;*
L_2 is the distance traveled by the material sphere along the horizontal plate, *mm.*
θ_2 is the angle between the two test platforms, (°)

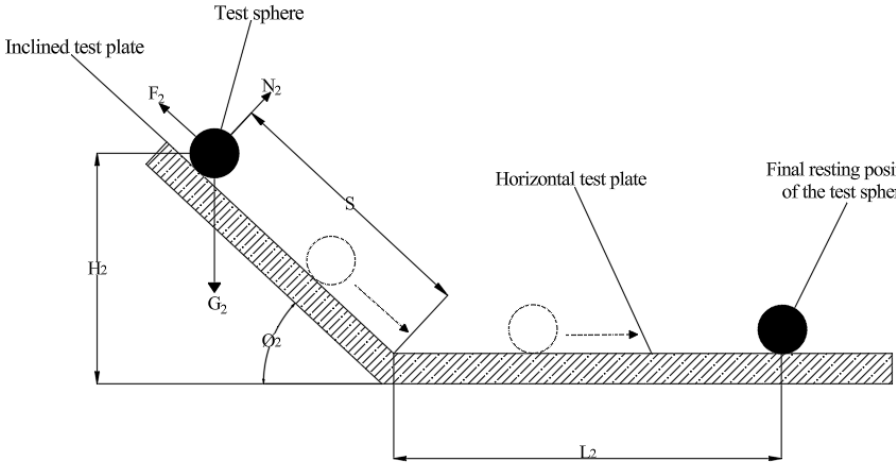

Fig. 4 – Principle of measuring the coefficient of rolling friction

Construction of the Discrete Element Model

Discrete Element Model of Lateritic Soil

Particle size distribution was determined using the standard sieve analysis method. The test equipment consisted of a set of standard sieves (with aperture sizes of 0.15 mm, 0.5 mm, 1 mm, 2 mm, and 3.5 mm) and an electronic balance (accuracy: 0.01 g). Sieve analysis was performed with a consistent shaking duration of 10 minutes. After shaking, the lateritic soil particles retained on each sieve were weighed. The test was repeated three times, with measurements recorded to an accuracy of 0.1 g. The lateritic soil particles after sieving are shown in Figure 5.

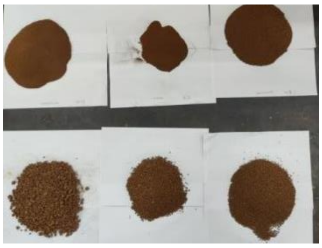

Fig. 5 – Particles after sieving

Based on the fundamental theory of the discrete element method (*DEM*) and the assumption of medium continuity, the macroscopic mechanical behavior of a granular system is essentially governed by the microscopic contact network and interaction forces between particles (*Cundall P.A. et al., 1979*). Through dimensional analysis and similarity principles, an upscaled model can equivalently reproduce macroscopic rheological and mechanical properties while reducing particle count and enhancing simulation feasibility. Currently, there is no unified standard for soil particle modeling based on the discrete element method (*DEM*). Spherical particles with diameters of 4–6 mm are commonly employed in studies (*Hang et al., 2018; Ucgul et al., 2015*). To balance efficiency and authenticity, this study adopts a five-fold coarse-graining technique and generates particles proportionally by mass fraction to ensure consistent particle size distribution. The corresponding mass fraction settings are shown in Table 1.

Table 1

Diameter and Mass Distribution of EDEM-Simulated Red Clay Particles

Actual particle size [mm]	Simulated particle diameter [mm]	Mass fraction [%]
≤0.25	0.625	22.4
0.25-0.5	1.875	11.8
0.5-1	3.250	19.4
1-2	7.500	19.8
2-3	12.500	20.6
≥3	15.000	6.0

Considering both simulation accuracy and modeling efficiency, particles were appropriately scaled up and then consolidated in shape. For particles smaller than 0.5 mm, the default spherical model in EDEM was adopted; for particles ranging from 0.5 mm to 2 mm, a two-ball model in EDEM was employed; and for particles larger than 2 mm, a three-ball model in EDEM was used. The established model is shown in Fig. 6.

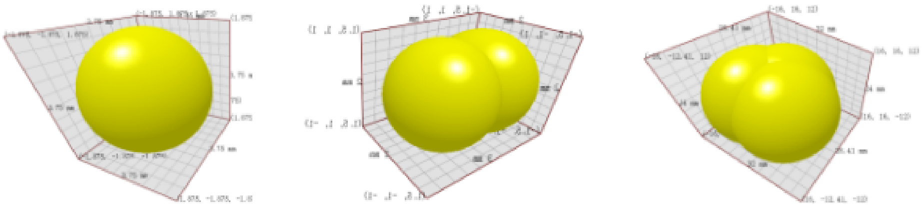

Fig. 6 – Establishment of Simulated Red Clay Particles

Discrete Element Model of Panax notoginseng (DEM)

The key physical parameters of *P. notoginseng* seedlings were determined for construction of the DEM. The morphological structure and principal dimensions of a representative seedling are shown in Fig. 7.

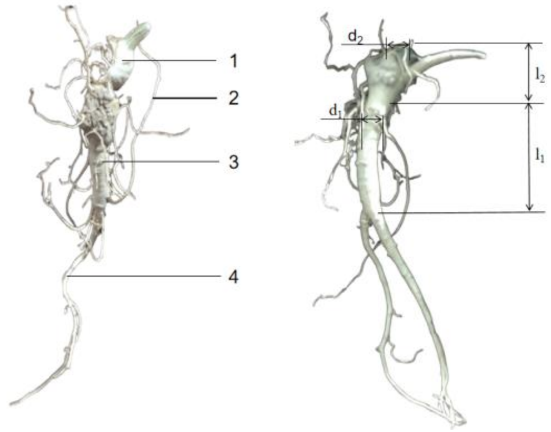

Fig. 7 – *P. notoginseng* seedling

1.dormant bud (rhizome head) 2. lateral root 3. main root 4. fibrous root

Two hundred *P. notoginseng* seedlings were selected for measurement, and their dimensional parameters are presented in Table 2.

Table 2

Dimensional parameters of *P. notoginseng* seedlings

Parameter	Main root length l_1[mm]	Main root diameter d_1[mm]	Dormant bud length l_2[mm]	Dormant bud diameter d_2[mm]
maximum value	26.12	15.68	17.74	8.89
minimum value	17.50	9.08	8.38	4.35
average value	22.42	12.64	13.28	6.15

High-precision point cloud data of *P. notoginseng* seedlings were acquired using the Wiiboox Reeyee 3D scanner, and a digital twin model with realistic topological structure was constructed through reverse engineering technology, overcoming the limitations of traditional contact measurement methods in characterizing the geometric features of complex biological samples (*Tang et al., 2023; Zhao et al., 2023*), as shown in Figure 8.

Fig. 8 – Wiiboox Reeyee 3D scanner

The model was imported into Creo Parametric 2.0, where the biologically characteristic surfaces were mathematically reconstructed by optimizing the control points and imposing surface-continuity constraints. To reduce the computational burden and simulation time, the *P. notoginseng* seedling model was simplified by retaining only the main root structure. The modeling procedure and resulting model are shown in Fig. 9.

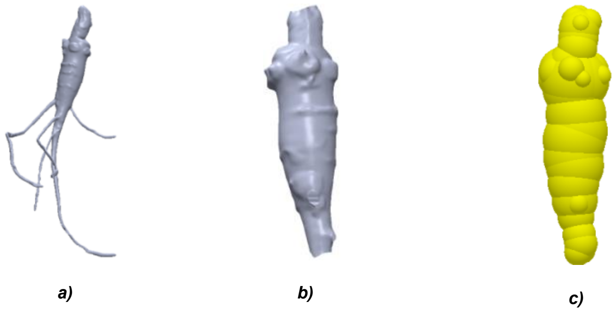

Fig. 9 – Modeling process of *P. notoginseng* seedling
a) 3D Scanning File; b) Simplified Contour Model; c) Seedling Simulation Model

Experiment and Simulation

Determination of Simulation Parameters

In the EDEM simulation of interaction processes, the contact parameters include the coefficient of restitution (C_R), coefficient of static friction (S_F), coefficient of rolling friction (R_F), and surface energy (S_E) between materials. This study focused on the contact parameters of the implement–lateritic soil – *P. notoginseng* interaction system during transplantation. These parameters included the following: for lateritic soil–lateritic soil, the coefficient of restitution (C_{R1}), static friction coefficient (S_{F1}), rolling friction coefficient (R_{F1}), and surface energy (S_{E1}); for lateritic soil–*P. notoginseng*, the coefficient of restitution (C_{R2}), coefficient of static friction (S_{F2}), coefficient of rolling friction (R_{F2}), and surface energy (S_{E2}); and for lateritic soil–65Mn steel, the coefficient of restitution (C_{R3}), coefficient of static friction (S_{F3}), coefficient of rolling friction (R_{F3}), and surface energy (S_{E3}). The intrinsic parameters and contact parameters were obtained through physical experiments and relevant literature (*Yu et al., 2020; Zhang et al., 2025; Liu et al., 2025*), as listed in Table 3.

Table 3

Ranges of intrinsic material properties and contact parameters

Parameter	Lateritic soil	*P. notoginseng*	65Mn
Density [kg/m^3]	1900	1050	7865
Young's modulus [Pa]	7.8e+06	2.29e+06	7.27e+10
Poisson's Ratio	0.370	0.402	0.35
Coefficient of restitution with lateritic soil	0.06-0.15	0.1-0.5	0.2-0.6
Coefficient of static friction with lateritic soil	0.1-0.6	0.2-0.6	0.1-0.55
Coefficient of rolling friction with lateritic soil	0.05-0.3	0.1-0.5	0.04-0.12
JKR surface energy with lateritic soil [J/m^2]	2-8	2-5	1-5

Development of Calibration Experiments for the Discrete Element Simulation

Calibration experiments for the lateritic soil–lateritic soil contact parameters were conducted using a Box–Behnken design. The mean natural angle of repose of the lateritic soil, denoted as C_{S1} was selected as the response variable to evaluate the effects and statistical significance of the four factors C_{R1}, S_{F1}, R_{F1}, and S_{E1}. After each simulation, images of the soil pile were captured from the ±*X* and ±*Y* directions, as shown in Figure 10.

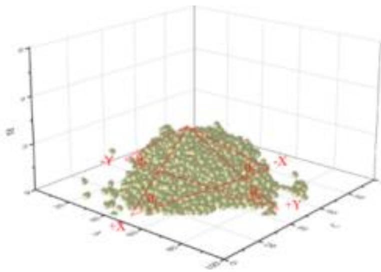

Fig. 10 - Cross-section selection

Calibration simulations for the lateritic soil–*P. notoginseng* contact parameters were conducted using a Box–Behnken design. The angle of repose of the lateritic soil–*P. notoginseng* mixture, denoted as C_{S2} was selected as the response variable to evaluate the effects and statistical significance of C_{R2}, S_{F2}, R_{F2}, and S_{E2}. As shown in Fig. 11, the mixture was placed in the test container, after which the bottom support plate was withdrawn. Once the material had stabilized, image processing and linear fitting were performed to determine the angle of repose. The mean measured angle was used as the simulation response.

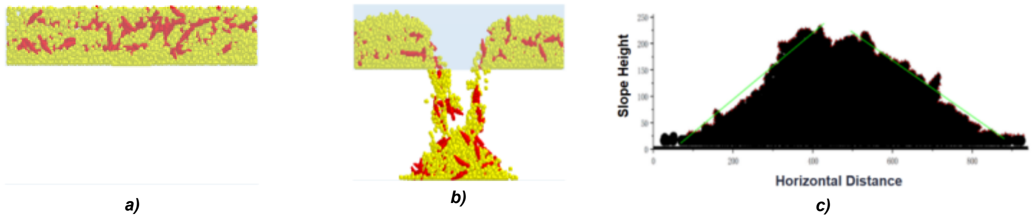

Fig. 11 – Mixture Collapsing Test

a) Laterite-P. notoginseng mixture uniformly distributed; b) Mixture Collapsing; c) Experimental Image Processing

The calibration test for simulation parameters between lateritic soil and 65Mn steel was conducted using an inclined plane simulation with a Box-Behnken design, as shown in Figure 12. A particle factory was set parallel to the inclined plane to generate a 15 mm-diameter soil sphere, which was initialized tangent to the surface with zero initial velocity and allowed to slide naturally, with its sliding distance on the horizontal plane (C_{S3}) recorded as the response value to investigate the effects and significance of the coefficient of restitution (C_{R3}), coefficient of static friction (S_{F3}), coefficient of rolling friction (R_{F3}), and surface energy (S_{E3}).

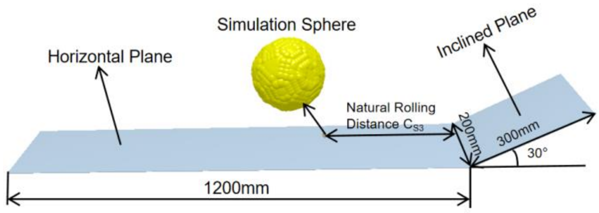

Fig. 12 – Inclined Plane Simulation

Results of Box-Behnken Simulation Calibration Experiments

Analysis of variance (*ANOVA*) was performed on the Box-Behnken experimental results for the lateritic soil–lateritic soil contact parameters, as shown in Table 4. After removing the non-significant terms with P > 0.05 from the ANOVA, the final predictive model for the response value under the lateritic soil–lateritic soil contact parameters was obtained as follows:

$$C_{S1} = 39.9 + 1.51R_{F1} + 7.63S_{E1} + 0.475C_{R1}S_{E1} + 2.18S_{F1}S_{E1} + 3.37C_{R1}^2 - 1.08C_{R1}S_{F1} - 0.725R_{F1}S_{E1} - 0.6417S_{F1}^2 - 0.9917R_{F1}^2 + 0.5708S_{E1}^2 \quad (4)$$

Table 4

Analysis of variance (ANOVA) for Laterite—Laterite parameter experiments

Source of Variance	Sum of Squares (SS)	Degrees of Freedom (df)	Mean Square (MS)	F	P
Model	861.69	14	61.55	295.34	< 0.0001
C_{R1}	0.0000	1	0.0000	0.0000	1.0000
S_{F1}	0.5208	1	0.5208	2.50	0.1399
R_{F1}	27.30	1	27.30	131.00	< 0.0001
S_{E1}	699.21	1	699.21	3355.1	< 0.0001
$C_{R1}S_{F1}$	4.62	1	4.62	22.18	0.0005
$C_{R1}R_{F1}$	0.9025	1	0.9025	4.33	0.0595
$C_{R1}S_{E1}$	10.24	1	10.24	49.14	< 0.0001
$S_{F1}R_{F1}$	0.3025	1	0.3025	1.45	0.2515
$S_{F1}S_{E1}$	18.92	1	18.92	90.80	< 0.0001
$R_{F1}S_{E1}$	2.10	1	2.10	10.09	0.0080
C_{R1}^2	60.60	1	60.60	290.78	< 0.0001
S_{F1}^2	2.20	1	2.20	10.54	0.0070
R_{F1}^2	5.24	1	5.24	25.17	0.0003
S_{E1}^2	1.74	1	1.74	8.34	0.0136
Lack of Fit	2.36	10	0.2361	3.37	0.2503
Total	864.19	26			

Analysis of variance (*ANOVA*) was conducted on the Box-Behnken experimental results for the lateritic soil–*P. notoginseng* contact parameters, and the results are presented in Table 5. After removing non-significant terms with P > 0.05 from the analysis, the final prediction model for the natural collapse coefficient C_{S2} under the lateritic soil–*P. notoginseng* contact parameters was obtained as follows:

$$C_{S2}=37.97+3.78S_{F2}+4.7R_{F2}+3.08S_{E2} +0.85R_{F2}S_{E2}+0.475S_{F2}^{2}-0.3125S_{E2}^{2} \quad (5)$$

Table 5

Analysis of variance (ANOVA) for Laterite-*P. notoginseng* parameter experiments

Source of Variance	Sum of Squares (SS)	Degrees of Freedom (df)	Mean Square (MS)	F	P
Model	556.81	14	39.77	422.05	< 0.0001
C_{R2}	0.1408	1	0.1408	1.49	0.245
S_{F2}	171.01	1	171.01	1814.67	< 0.0001
R_{F2}	265.08	1	265.08	2812.93	< 0.0001
S_{E2}	114.08	1	114.08	1210.61	< 0.0001
$C_{R2}S_{F2}$	0.4225	1	0.4225	4.48	0.0558
$C_{R2}R_{F2}$	0.09	1	0.09	0.955	0.3477
$C_{R2}S_{E2}$	0.01	1	0.01	0.1061	0.7502
$S_{F2}R_{F2}$	0.04	1	0.04	0.4245	0.527
$S_{F2}S_{E2}$	0.01	1	0.01	0.1061	0.7502
$R_{F2}S_{E2}$	2.89	1	2.89	30.67	0.0001
C_{R2}^2	0.4033	1	0.4033	4.28	0.0608
S_{F2}^2	1.2	1	1.2	12.77	0.0038
R_{F2}^2	0.0208	1	0.0208	0.2211	0.6467
S_{E2}^2	0.5208	1	0.5208	5.53	0.0367
Lack of Fit	0.9242	10	0.0924	0.8944	0.6354
Total	557.94	26			

Analysis of variance (*ANOVA*) was conducted on the Box-Behnken experimental results for the lateritic soil–65Mn steel contact parameters, and the results are presented in Table 6. After removing non-significant terms with P > 0.05 from the analysis, the final prediction model for the sliding distance C_{S3} under the lateritic soil–65Mn steel contact parameters was obtained as follows:

$$C_{S3}=407-3.5S_{F3}-162.42R_{F3}-80.08S_{E3}- 33.5S_{F3}R_{F3}-27.5R_{F3}S_{E3}+34.38R_{F3}^{2}+27.63S_{E3}^{2} \quad (6)$$

Table 6

Experimental design and results for Laterite—65Mn contact parameter calibration

Source of Variance	Sum of Squares (SS)	Degrees of Freedom (df)	Mean Square (MS)	F	P
Model	4.12E+05	14	29395.45	1014.36	< 0.0001
C_{R3}	65.33	1	65.33	2.25	0.1591
S_{F3}	147	1	147.00	5.07	0.0438
R_{F3}	3.17E+05	1	3.17E+05	10923.3	< 0.0001
S_{E3}	76960.08	1	76960.08	2655.7	< 0.0001
$C_{R3}S_{F3}$	1.0000	1	1.0000	0.0345	0.8557
$C_{R3}R_{F3}$	12.25	1	12.25	0.4227	0.5278
$C_{R3}S_{E3}$	6.25	1	6.25	0.2157	0.6507
$S_{F3}R_{F3}$	4489	1	4489	154.9	< 0.0001
$S_{F3}S_{E3}$	9.0000	1	9.0000	0.3106	0.5876
$R_{F3}S_{E3}$	3025	1	3025	104.39	< 0.0001
C_{R3}^2	0.3333	1	0.3333	0.0115	0.9164
S_{F3}^2	3.0000	1	3.0000	0.1035	0.7532
R_{F3}^2	6302.08	1	6302.08	217.47	< 0.0001
S_{E3}^2	4070.08	1	4070.08	140.45	< 0.0001
Lack of Fit	291.75	10	29.18	1.04	0.5844
Total	4.12E+05	26			

Analysis of Simulation Results and Optimal Combination of Contact Parameters

Quadratic multiple regression fitting and analysis of variance (*ANOVA*) were performed on the experimental data of the three contact interfaces using Design-Expert software. The ANOVA results revealed significant interaction effects among the factors, and 3D response surfaces were plotted for the factors with significant interactions, as shown in Figure 13.

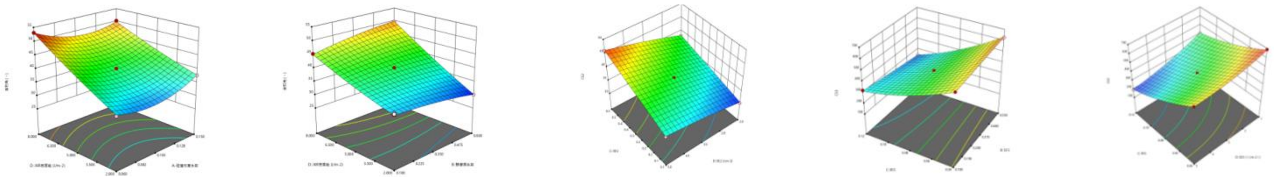
a） b） c） d) e)

Fig. 13 – 3D response surface of significant factors on C_S

The regression models were solved via Design-Expert optimization, targeting the experimental values: a lateritic soil angle of repose of 41.2°, a mixture collapse angle of 45.2°, and a natural sliding distance of 423 mm. After simulation verification (Figure 14), the parameter combinations closest to the measured data were selected as optimal solutions. For the lateritic soil–lateritic soil interface, the optimal parameters were a rolling friction coefficient of 0.287 and a JKR surface energy of 5.302 J/m², with non-significant factors (static friction coefficient 0.575, coefficient of restitution 0.11) set to average experimental values. For the lateritic soil–*P. notoginseng* interface, the optimal parameters were: coefficient of restitution 0.157, coefficient of static friction 0.482, coefficient of rolling friction 0.124, and JKR surface energy 4.101 J/m². For the lateritic soil–65Mn steel interface, the optimal parameters were a coefficient of static friction of 0.42, a coefficient of rolling friction of 0.09, and a JKR surface energy of 3.806 J/m², with the non-significant coefficient of restitution set to 0.13.

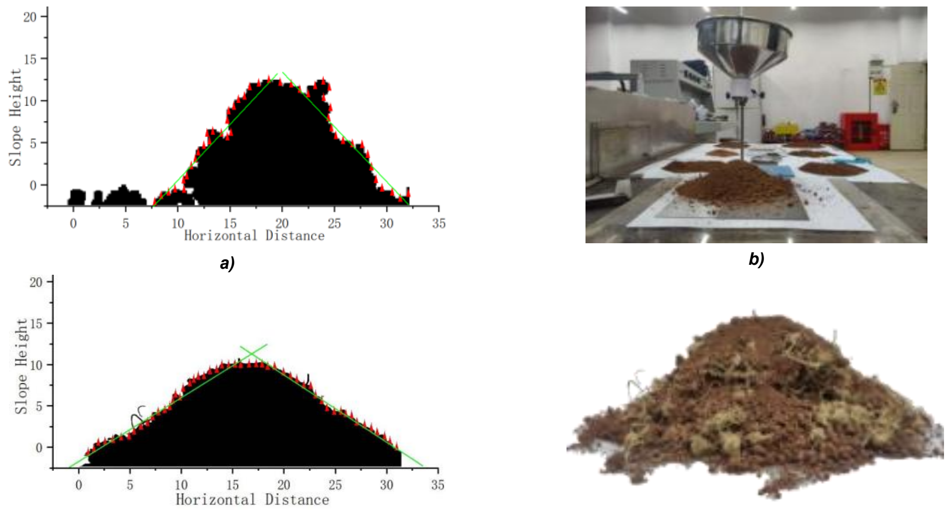

a) b) c) d)

Fig. 14 – Comparison between Simulation Results and Physical Experimental Results

a) Binarization Processing of Simulation Results; b) Physical Experiment of Laterite Accumulation; c) Binarization Processing of Physical Collapsing Test; d) Mixture Collapsing Test

Interactive Simulation Validation

Dynamic Bench-Test Validation

A drum-test simulation based on the discrete element method (DEM) was conducted using EDEM. As shown in Fig. 15, the 65Mn steel drum had a diameter of 300 mm and a height of 80 mm and was uniformly filled with a mixture of *P. notoginseng* and lateritic soil. Three comparative tests were conducted at drum rotational speeds of 60, 90, and 120 r/min, with rotational speed as the only variable. After each simulation, four representative stages were compared: initial material lifting, critical slippage, the first complete circulation cycle, and stable dynamic flow. The analysis included measuring the tangential angle between the material bed and the inner drum wall at the three-quarter lifting position; recording the time from initial lifting to critical slippage; comparing the binarized contours obtained during the first circulation cycle with those from the physical test at the corresponding time point; and measuring the material-distribution length during stable flow to compare it with the stratification observed in the physical tests.

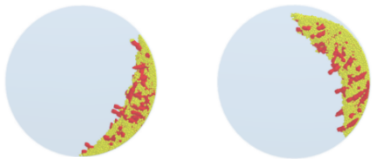
a) b)

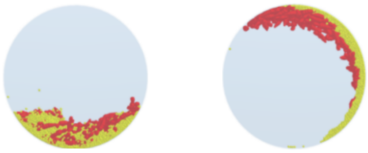
c) d)

Fig. 15 – Four key moments of the mixture

a) initial material lifting; b) critical slippage; c) the first complete accumulation cycle; d) stable dynamic flow

The motion of the materials inside the drum was recorded using a high-speed imaging system, as shown in Fig. 16. The drum dimensions and material properties were consistent with those used in the simulation model.

Tests were conducted at drum rotational speeds of 60, 90, and 120 r/min. Images of the material behavior at four representative stages were captured, and a quantitative comparison between the physical tests and simulation results is presented in Table 12. The relative error in the initial material-lifting angle was 4.33%, the relative error in the time from initial lifting to critical slippage was 4.06%, the contour-overlap rate during the first circulation cycle was 93.3%, and the relative error in the material-distribution length during the stable-flow stage was 2.79%.

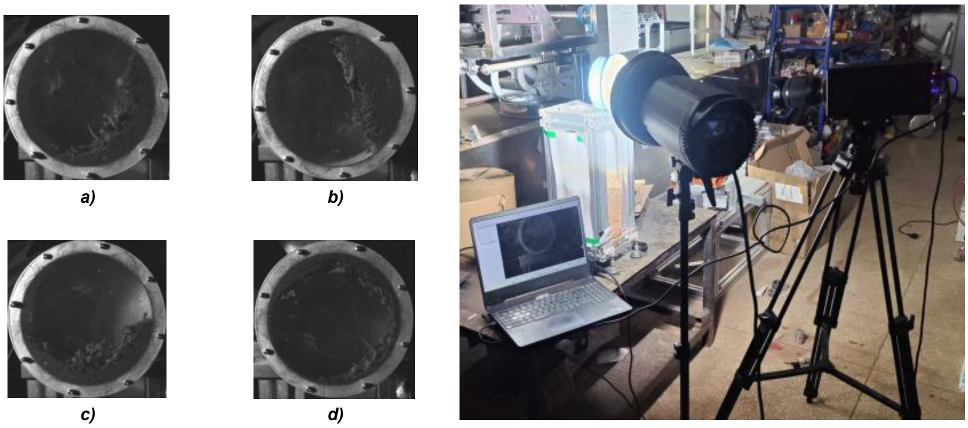
a) b) c) d) e)

Fig. 16 – Physical rotary-drum experiment

a) initial material lifting; b) critical slippage; c) first complete accumulation cycle;
d) stable dynamic flow; e) high-speed image acquisition

Field validation test

A discrete element simulation of the ditching operation was conducted using EDEM, as shown in Fig. 17. The soil bin measured 2.0 m in length, 1.5 m in width, and 0.4 m in height. With the forward speed of the ditching tool as the only variable, three comparative simulations were conducted at 3, 9, and 15 m/min. The simulation used the optimized physical properties of the lateritic soil and the tool–soil contact parameters determined in the preceding study. After each simulation, the top diameter of the ditching hole, *x*, and the hole depth, *y*, were measured consistently.

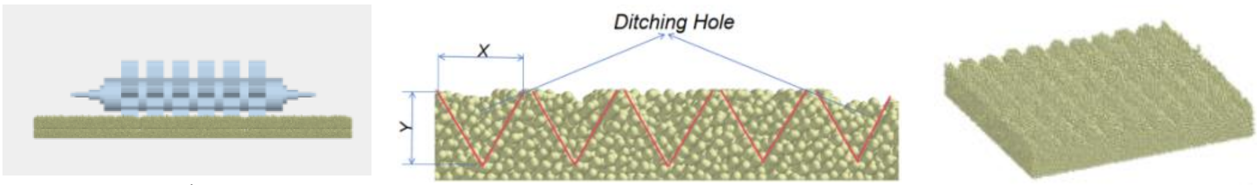

a) b) c)

Fig. 17 – Ditching Simulation

a) Ditching Simulation; b) Simulation Results and Measurement Principle; c) Soil Mass After Ditching

A field ditching test was conducted using a pitting roller with a length of 842 mm, a shaft diameter of 220 mm, and a tooth height of 50 mm, as shown in Fig. 18.

a) b)

Fig. 18–Results of Field Experiment

a) Field ditching result; b) Field test

The forward speed of the implement was set at three levels: 3, 9, and 15 m/min. After each test, the top diameter of the pit, *x*, and the pit depth, *y*, were measured at five randomly selected locations, and the mean values were calculated. The mean relative errors between the simulated and field-measured values were 3.52% for the pit-top diameter and 4.28% for the pit depth. The comparison between the simulation and physical-test results is presented in Table 7.

Table 7

Comparison of simulation and physical-test results

Operating condition	Evaluation parameter	Simulated result	Measured result	Relative error
Drum speed at 60 r/min; implement speed at 3 m/min.	Initial material-lifting angle [°]	42.8	44.7	4.27%
	Time to critical slippage [ms]	124	128	3.13%
	Material-distribution length during stable flow [mm]	565	550	2.72%
	First complete accumulation stage [mm]	-	-	7.23%
	Pit-top diameter [mm]	36.6	34.3	3.79%
	Pit depth [mm]	41.8	40.2	3.98%
Drum speed at 90 r/min; implement speed at 6 m/min.	Initial material-lifting angle [°]	40.3	42.2	4.50%
	Time to critical slippage [ms]	179	187	4.28%
	Material-distribution length during stable flow [mm]	659	642	2.65%
	First complete accumulation stage	-	-	6.18%
	Pit-top diameter [mm]	36.2	34.5	2.86%
	Pit depth [mm]	40.8	39.2	4.08%
Drum speed at 120 r/min; implement speed at 9 m/min.	Initial material-lifting angle [°]	36.3	37.9	4.22%
	Time to critical slippage [ms]	198	208	4.76%
	Material-distribution length during stable flow [mm]	754	732	3.00%
	First complete accumulation stage	-	-	6.68%
	Pit-top diameter [mm]	34.6	33.3	3.90%
	Pit depth [mm]	38.4	36.6	4.79%

CONCLUSIONS

Three Box-Behnken experiments were conducted to systematically evaluate the relationships between contact parameters and the response variables (C_{S1}, C_{S2}, C_{S3}). The significant factors were identified as follows: R_{F1} and S_{E1} for C_{S1}; S_{F2}, R_{F2}, and S_{E2} for C_{S2}; and R_{F3} and S_{E3} for C_{S3}.

Response surface analysis was then performed using C_{S1}, C_{S2}, and C_{S3} as the response variables to optimize the significant contact parameters associated with each response. The nonsignificant parameters were assigned the mean values obtained from the physical experiments. The optimal parameter combinations were determined as follows: S_{E1}=5.302 J/m², R_{F1}=0.287; S_{E2}=4.101 J/m², S_{F2}=0.482, R_{F2}=0.124; S_{E3}=3.806 J/m², S_{F3}=0.42, R_{F3}=0.09. The corresponding nonsignificant parameters were set to: C_{R1}=0.11, S_{F1}=0.575; C_{R2}=0.157; C_{R3}=0.13.

Comparison of the simulation and physical-test results showed a high degree of agreement under all test conditions, including different drum rotational speeds and implement forward speeds. The relative errors for all evaluated indicators, including pit depth and mixture behavior at four representative stages, were below 7.5%, with a maximum value of 7.23%. This close agreement confirmed the accuracy and reliability of the calibrated parameters used in the discrete element interaction model. The resulting model therefore provides a reliable parameter basis for subsequent simulation and optimization of the operating process of the *P. notoginseng* transplanting machine.

REFERENCES

[1] Aikins, K.A., Ucgul, M., Barr, J.B. (2021). Determination of discrete element model parameters for a cohesive soil and validation through narrow point opener performance analysis. *Soil and Tillage Research*, Vol 213, pp. 105123.

[2] Adajar, J.B., Alfaro, M., Desses, P. (2021). Calibration of discrete element parameters of crop residues and their interfaces with soil. *Computers and Electronics in Agriculture*, Vol 188, pp. 106340.

[3] Aikins, K. A., Ucgul, M., Barr, J. B. (2021). Determination of discrete element model parameters for a cohesive soil and validation through narrow point opener performance analysis. *Soil and Tillage Research*, Vol 213, pp. 105123.

[4] Bahrami, M., Naderi - Boldaji, M., Ghanbarian, D., Ucgul, M., Keller, T. (2020). Simulation of plate sinkage in soil using discrete element modelling: calibration of model parameters and experimental validation. *Soil and Tillage Research*, Vol 203, pp. 104700.

[5] Cundall, P.A., Strack, O.D.L. (1979). A discrete numerical model for granular assemblies. *Geotechnique*, Vol 29(1), pp. 47 - 65.

[6] Hang, C., Gao, X., Yuan, M.L. (2018). Discrete element simulations and experiments of soil disturbance as affected by the tine spacing of subsoiler. *Biosystems Engineering*, Vol 168, pp. 73 - 82.

[7] Liu, L. H., Liu, Y., Wang, F., Liu, S.L., Hu, H.Z., Zhang, W.S., Xin, W.F. (2017). Current situation and development suggestions of the Panax notoginseng industry in Yunnan (云南三七产业发展现状及发展建议). *China Journal of Modern Chinese Medicine*, Vol 19, pp. 1331 - 1335.

[8] Li, J. W., Tong, J., Hu, B., Wang, H.B., Mao, C.Y., Ma, Y.H. (2019). Calibration of discrete element simulation parameters for the interaction between heavy clay black soil with different moisture contents and soil - contacting components (不同含水率黏重黑土与触土部件互作的离散元仿真参数标定). *Transactions of the Chinese Society of Agricultural Engineering*, Vol 35(6), pp. 130 - 140.

[9] Liu, W. Z., Huang, X. J., Xu, Y., Li, H. L., Wan, J. L. (2025). Research on the cumulative deformation law and control of compacted red clay under dynamic wetting (动力湿化作用下压实红黏土累积变形规律与控制研究). *Chinese Journal of Geotechnical Engineering*, Vol 47(03), pp. 535 - 547.

[10] Shao, M. A., Wang, Q. J., Huang, M. B. (2006). Soil Physics (土壤物理学). *Beijing: Higher Education Press.*

[11] Shi, R.J., Dai, F., Zhao, W.Y., Zhang, F., Shi, L., Guo, J. (2022). Establishment of a discrete element flexible model for flax stalks and experimental verification of contact parameters (胡麻茎秆离散元柔性模型建立与接触参数试验验证). *Transactions of the Chinese Society for Agricultural Machinery*, Vol 53(10), pp. 146 - 155.

[12] Tang, J. (2023). The shape parameters of coal and gangue particles derived from 3D scanning. *Scientific Data*, Vol 10(1), pp. 1 - 7.

[13] Tian, X. L., Cong, X., Qi, J. T., Guo, H., Li, M., Fan, X. H. (2021). Parameter calibration of the discrete element model for corn straw - soil mixture in black soil area (黑土区玉米秸秆 - 土壤混料离散元模型参数标定). *Transactions of the Chinese Society for Agricultural Machinery*, Vol 52(10), pp. 100 - 108 + 242.

[14] Ucgul, M., Fielke, J. M., Saunders, C. (2015). Three - dimensional discrete element modelling (DEM) of tillage: accounting for soil cohesion and adhesion. *Biosystems Engineering*, Vol 129, pp. 298 - 306.

[15] Xing, J. J., Zhang, R., Wu, P., Zhang, X., Dong, X., Chen, Y., Ru, S. (2020). Parameter calibration of discrete element simulation model for latosol particles in Hainan tropical area (海南热区砖红壤颗粒离散元仿真模型参数标定). *Transactions of the Chinese Society of Agricultural Engineering*, Vol 36(5), pp. 158 - 166.

[16] Xiang, W., Wu, M. L., Lü, J. N., Quan, W., Ma, Lan, Liu, J. J. (2019). Calibration of simulation physical parameters of cohesive loam based on stacking test (基于堆积试验的黏壤土仿真物理参数标定). *Transactions of the Chinese Society of Agricultural Engineering*, Vol 35(12), pp. 116 - 123.

[17] Yang, K., Yang, L., Fan, W. (2019). Illumina - based transcriptomic analysis on recalcitrant seeds of Panax notoginseng for the dormancy release during the after - ripening process. *Physiologia Plantarum*, Vol 167(4), pp. 597 - 612.

[18] You, Q., Yang, Q. L. (2022). Effects of different drainage bodies on the growth of Panax notoginseng, soil nutrients and soil microorganisms in the root zone (不同排水体对三七生长、土壤养分及根区土壤微生物的影响). *Journal of Drainage and Irrigation Machinery Engineering*, Vol 40(9), pp. 959 - 965.

[19] Yunnan Provincial Administration for Market Regulation. (2020). DB53/T 055.3 - 2020 Panax notoginseng seedlings (三七种苗). *Kunming: Yunnan Provincial Administration for Market Regulation*.

[20] Yu, Q. X., Liu, Y., Chen, X. B., Sun, K., Lai, Q. H. (2020). Calibration and experiment of simulation parameters for Panax notoginseng seeds based on the discrete element method (基于离散元的三七种子仿真参数标定与试验). *Transactions of the Chinese Society for Agricultural Machinery*, Vol 51(02), pp. 123 - 132.

[21] Zeng, Z.W., Ma, X., Cao, X.L., Li, Z., Luo, X.. (2021). Application status and prospects of the discrete element method in agricultural engineering research (离散元法在农业工程研究中的应用现状和展望). *Transactions of the Chinese Society for Agricultural Machinery*, Vol 52(4), pp. 1 - 20.

[22] Zhang, R. F., Zhou, J. L., Liu, H., Shi, S., Wei, G. J., & He, T. F. (2022). Research on the calibration method of discrete element simulation parameters for the corn particle bonding model (玉米颗粒粘结模型离散元仿真参数标定方法研究). *Transactions of the Chinese Society for Agricultural Machinery*, Vol 53(Suppl 1), pp. 69 - 77.

[23] Zhao, J. W. (2022). Design and experiment of a pneumatic directional transplanting device for Panax notoginseng seedlings (气力式三七种苗定向移栽装置设计与试验). *Kunming University of Science and Technology.*

[24] Zhang, H.D., Tang, Z.X., Zhang, L.Y. (2025). Optimization of Discrete Elemental Simulation Parameters for Forest Panax pseudoginseng Plantation Red Soil Based on GA - BP - GA. *Journal of Agricultural Science and Technology*, Vol 27(9), pp. 120 - 130.